

Performance of an electrical distribution network with Soft Open Point during a grid side AC fault



Avinash Aithal^a, Gen Li^a, Jianzhong Wu^{a,*}, James Yu^b

^a School of Engineering, Cardiff University, Cardiff CF24 3AA, UK

^b SP Energy Networks, Blantyre, Scotland G72 0HT, UK

HIGHLIGHTS

- Performance of a distribution network with SOP during an AC fault was investigated.
- Convectional fault analysis using sequence networks was extended to include SOP.
- Network behaviour was analysed for a line-ground, a line-line and a three-phase fault.
- A method to detect AC faults was developed using sequence voltage measurements.
- Dependence of sequence voltages and currents on SOP set-points was investigated.

ARTICLE INFO

Keywords:

Electrical distribution network
Power electronics
Soft Open Points
Faults
Symmetrical components
Sequence network

ABSTRACT

Soft Open Point (SOP) is a power electronic device installed in place of normally open points in electrical distribution networks. This paper investigates the dynamic performance of a medium voltage (MV) distribution network with a connected SOP, under grid side AC faults. Use of sequence networks was extended to include SOP, such that conventional fault analysis technique can be used on a distribution network with SOP. A Fault-Index was defined using symmetrical components of voltages measured at the grid connection point of the SOP. The network performance was investigated under a line-to-ground, a line-to-line and a three-phase fault. The behaviour of the network was analysed under different control schemes and various operating scenarios of the SOP. Furthermore, the dependence of the sequence voltages and currents on the SOP set points was investigated. Simulations were carried out on an 11 kV generic UK distribution network model developed in PSCAD/EMTDC. Results show that the convectional fault analysis technique is applicable on a network with SOP, regardless of the SOP control mode. The Fault-Index, defined based on the local voltage measurements, was effective in detecting the presence of an AC fault in the MV distribution network. In addition, the need for a non-current based detection method is illustrated.

1. Introduction

In medium voltage (MV) distribution networks, power electronic devices have been increasingly deployed due to their applications in integrating distributed energy resources (DER) [1]. Applications of power electronic devices such as electronic on-load tap changers, solid state fault current limiters and Soft Open Points (SOPs) are mainly under investigation [2,3]. This paper focuses on SOP used in medium voltage distribution networks.

SOP is a power electronic device installed in place of a normally open or normally closed point in a distribution network [4,5]. Unlike conventional switches, the power flow through an SOP is not controlled through open and close operation of mechanical contactors. Controlled

firing of power electronic switches performs ‘soft’ switching. The desired steady state operation is achieved by regulating the real (P) and reactive (Q) power flowing through the SOP terminals.

An MV distribution network normally operates in a radial configuration. An SOP connects two radial networks retaining the benefits of the radial and the meshed configurations, whilst avoiding their individual drawbacks [6]. Loads may be balanced between feeders without increasing the fault level of an individual radial feeder [7]. An algorithm to implement network reconfiguration with SOP was proposed in [8]. A method was introduced to determine the optimal SOP operation using an improved Powell’s direct set method. Authors of paper [4] proposed a method to determine the optimal installation sites and capacities of SOPs under normal operating conditions. A mixed

* Corresponding author.

E-mail address: wuj5@cardiff.ac.uk (J. Wu).

<http://dx.doi.org/10.1016/j.apenergy.2017.08.152>

Received 30 January 2017; Received in revised form 27 July 2017; Accepted 13 August 2017

Available online 21 August 2017

0306-2619/© 2017 The Author(s). Published by Elsevier Ltd. This is an open access article under the CC BY license

(<http://creativecommons.org/licenses/by/4.0/>).

integer non-linear optimization problem was formulated based on the typical operation scenarios generated by Wasserstein distance. The steady state operation of an SOP and the network restoration after a permanent fault using SOP were investigated in [9]. The authors presented various operation modes of an SOP during normal network conditions and further investigated the ‘restoration mode’ after fault isolation. Applications of SOP for load balancing and voltage profile management have been investigated in [8,10]. A steady state analysis framework was introduced in [11] to quantify the benefits of SOP in normal operation. The optimal operation of MV networks with distribution generation based on the Jacobean matrix sensitivity method was investigated in [12]. In [13], the authors investigated the impact of using an SOP on the feeder automation events on a distribution network. Distribution network operators (DNOs) in the UK such as the Scottish Power Energy Networks (SPEN) and the Western Power Distribution are deploying SOP-type equipment in their pilot projects [14,15]. However, the trials are in their early stage of development.

Existing literature mostly describes the behaviour and benefits of SOP under the normal network operation and the post fault scenarios. However, the existing literature does not describe the performance of a network with SOP during a fault on the network. No attempt has been seen to incorporate SOP into conventional fault analysis. To fill this gap, this paper extends the fault analysis technique using sequence networks to a distribution network with connected SOP.

A method was developed to detect faults in a distribution network with SOP, using sequence voltage measurements at the grid connection point of the SOP. A Fault-Index (*FI*) was defined to quantify the proportion of positive and negative sequence voltage at the SOP grid connection point. The presence of a fault in the network was determined by establishing a threshold of the *FI* value. A mechanism to detect faults is important to achieve proper operation of an SOP. Conventionally, separate fault management devices are used to detect the presence of a fault and disconnect the power electronic devices from the network during AC faults [16]. The method proposed in this paper is easy to implement since the inputs require only the local measurements at the grid connection point of the SOP. The efficacy of using the SOP for fault detection, as an alternative to conventional protection equipment, was investigated.

The sequence networks were verified by analysing the dynamic performance of a distribution network with SOP during a line-to-ground (L_a-G) fault, a line-to-line (L_a-L_b) and a three-phase ($L_a-L_b-L_c$) fault. The behaviour of the network was analysed under different control schemes and various operating scenarios of the SOP. Furthermore, the dependence of the sequence voltages and currents on the SOP set points was investigated.

2. Back-to-back voltage source converter based Soft Open Point

Various configurations of SOP are discussed in [6], which use back-to-back voltage source converters (VSCs), unified power flow controllers (UPFC), static series synchronous compensators (SSSC) or multi-terminal (MT) VSCs. Each configuration has a different operating region in the P-Q plane. Suitable configuration is selected based on network requirements.

Fig. 1(a) shows the operating region in the PQ plane for an SOP in back-to-back VSC configuration. The operating region is represented by a circle with its radius equal to the total rated apparent power (*S*) of the SOP. The VSC based SOP allows control of real and reactive power in all four quadrants of the P-Q plane. It can facilitate black start, unlike line commutated converters (LCC) [7]. It also injects reduced harmonic currents which allow the use of lighter filters. Furthermore, it has been suggested that back-to-back VSCs is the most cost effective configuration in distribution networks [3,5]. Therefore, an SOP using back-to-back VSC configuration is investigated in this paper.

The circuit topology of the SOP is shown in Fig. 1(b). It consists of two VSCs connected through a DC link. The VSC has six arms of

Insulated Gate Bipolar Transistors (IGBTs) connected in a bridge configuration. Each VSC is connected to the grid through an inductor and an isolation transformer. It is common to use two-level converters for lower voltage application (medium voltage or low voltage). Multilevel topologies are predominantly used for higher voltage levels [5].

2.1. Operation and modelling of SOP

Each VSC in the SOP is operated through controlled commutation of the IGBTs. Pulse width modulation (PWM) is used for the commutation. *P* transfer through the VSC is achieved by controlling the phase angles of the converter terminal voltage with respect to the SOP grid connection point. Transfer of reactive power (*Q*) is achieved by controlling the amplitude of voltage at the converter terminal with respect to the voltage at the SOP grid connection point. Smooth voltages are generated at the VSC terminals using low pass filters. The DC capacitors limit the ripples in DC current and provide for decoupled real power exchange between VSCs [17].

Fig. 2 shows the average model of an SOP. It is modelled using a switched equivalent of a VSC, with decoupled AC and DC sides. The AC side is modelled as a three-phase voltage source (V_1 for VSC1 and V_2 for VSC2). The DC side is modelled as a current source in parallel to a capacitor with the DC voltage V_{dc} . The direct current (I_{dc}) represents the real power transfer between the VSCs. The magnitudes of real power flowing between the terminals of SOP are equal during steady state operation. This is illustrated by the power balance equation in Eq. (1). P_1 and P_2 are the magnitudes of real power transferred across the terminals of the SOP. P_{dc} is the DC power transfer through the DC link.

$$P_1 = P_2 = P_{dc} = V_{dc} \times I_{dc} \quad (1)$$

The average model using switched equivalent circuit is sufficient for this study as it describes the steady state and the dynamic behaviour of the VSC with sufficient accuracy [18].

2.2. Control of SOP

A number of control schemes for VSCs have been proposed in the literature, including linear and non-linear methods [19–21]. A classical two-level *dq0*-control is used in this study [22]. It is a common control technique, since it allows the use of linear proportional-integral (PI) controllers to control the sinusoidal network quantities. This is achieved by transforming the three-phase (*a, b, c*) network quantities to a synchronously rotating reference frame (*d, q, 0*) using Parks transformation as shown in Eq. (2). $T(\theta)$ is the Park’s transformation matrix (details in Appendix A). X_{abc} is a vector of three-phase quantities in the *abc* frame. X_{dq0} is a vector of the converted quantities in the *dq0* frame.

$$[X_{dq0}] = [T(\theta)][X_{abc}] \quad (2)$$

The angle θ is synchronised to the grid angle using the angular frequency ω , obtained using a phase locked loop (PLL) [18]. ω is calculated using the positive sequence voltage as an input to the PLL. Details of symmetrical components are elaborated in Section 3.1. The angular frequency of the rotating frame is controlled such that the resultant θ maintains the quadrature axis voltage (V_q) at zero. The direct axis voltage (V_d) is linearly controlled to achieve the desired output.

Each VSC is equipped with a separate two-level cascaded control system, which includes an outer (power) and an inner (current) control loop as shown in Fig. 3. The outer loop uses PI controllers to regulate active power (*P*) or DC voltage (V_{dc}) through the direct axis variable and reactive power (*Q*) or AC voltage (*E*) through the quadrature axis variable. The outer loop produces the direct axis ($i_{d Ref}$) and the quadrature axis ($i_{q Ref}$) current reference signals for the inner loop.

The mode of operation is selected between the active power control (APC) and the direct voltage control (DVC) through switch $Sw1$. Similarly, the reactive power control (RPC) or the alternating voltage control (AVC) is selectable through switch $Sw2$. Therefore, the SOP

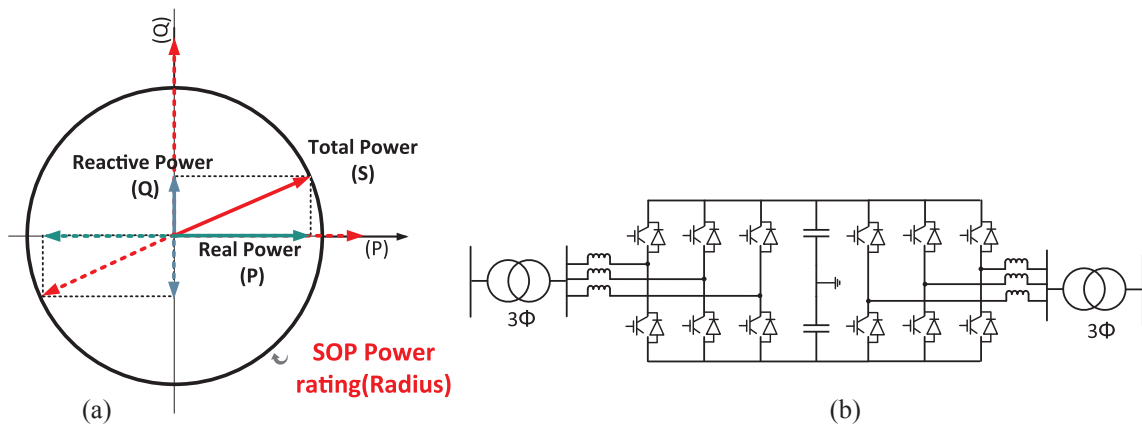


Fig. 1. (a) Operating region for VSC based SOP in P-Q plane; (b) IGBT connections for SOP implementation.

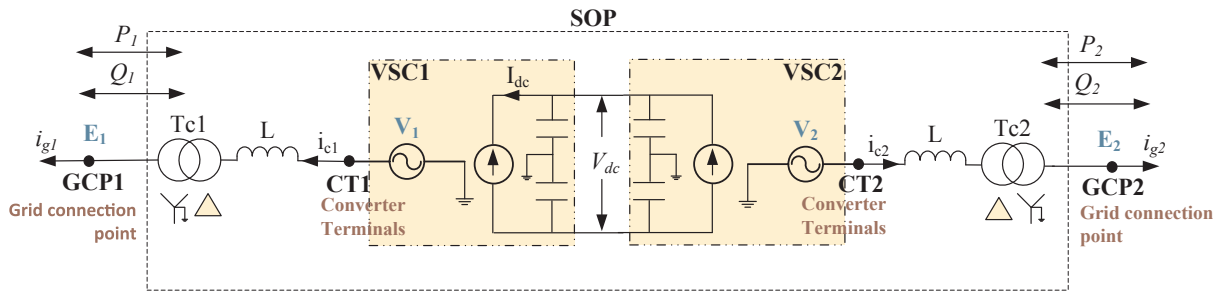


Fig. 2. Average model of an SOP.

control modes are switchable between the P-Q, V_{dc}-Q, V_{dc}-E and P-E modes.

The inner loop is used to regulate the values of the current references $i_{d Ref}$ and $i_{q Ref}$ received from the outer loop. Decoupling signals are included to eliminate cross-coupling dynamics. The summation of the inner loop PI controller outputs and the decoupling terms produces the direct and quadrature axis voltage references, $V_{d Ref}$ and $V_{q Ref}$ respectively. The voltage reference signals are then used to generate the converter terminal voltage (V_a, V_b, V_c) through an inverse Park's transformation. In the averaged model, the firing operation is realized through the functional equivalent of the IGBT operation. The modulation index m is defined using $V_{d Ref}$ and V_{dc} as shown in Eq. (3). Eqs. (4) and (5) show the mathematical implementation of the converter terminal voltages and the DC current flowing through the DC link [16]. $i_{a,b,c}$ are the AC current through phases a, b and c.

$$m = V_{d Ref} \left(\frac{2}{V_{dc}} \right) \quad (3)$$

$$V_k = m \left(\frac{V_{dc}}{2} \right); \text{ where } k = a, b, c \quad (4)$$

$$I_{dc} = \frac{m}{2} (i_a + i_b + i_c) \quad (5)$$

A sustained DC voltage ensures a balanced real power flow between the terminals of the SOP. Therefore, either VSC1 or VSC2 must control V_{dc} for proper operation of the SOP. However, both VSCs cannot control the DC link voltage simultaneously as this may lead to hunting [18]. Subscripts 1 and 2 are added to the variable names of the SOP to indicate values of VSC1 and VSC2 respectively. The reference values of the real power ($P_{1 Ref}$ and $P_{2 Ref}$), reactive power ($Q_{1 Ref}$ and $Q_{2 Ref}$) and the AC voltage ($E_{1 Ref}$ and $E_{2 Ref}$) at terminals of VSC1 and VSC2 are defined by the user as per network requirements. Any value within the

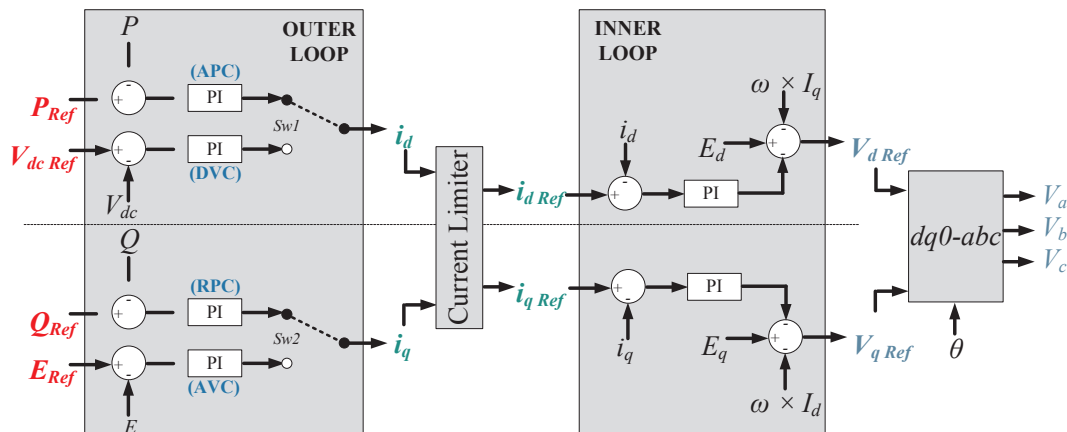


Fig. 3. Classical two-level cascaded control system of an SOP.

rating of the SOP is permissible. The DC voltage ($V_{dc Ref}$) is usually fixed for an SOP design. This study focuses on analysis of an SOP in combinations of P - Q and V_{dc} - Q modes only.

A current limiter is used to model the physical current carrying limitations of IGBTs. The maximum current through the SOP terminals (i_{max}) is assumed to be 1.5 times its rated current. Eq. (6) represents the mathematical implementation of the current limiter in the controller. This ensures that the IGBTs are protected from damage due to over-current.

$$(i_d)^2 + (i_q)^2 \leq (i_{max})^2 \quad (6)$$

3. Fault analysis of network with SOP using symmetrical components

3.1. Symmetrical components

Fortescue proposed the theory of symmetrical components in 1923 to study unbalanced networks [23]. During a fault, the unbalanced network can be resolved into three sets of balanced three-phase vector groups (positive, negative and zero sequences) called symmetrical components. Positive sequence components consist of balanced three-phase vectors in normal phase sequence. Vectors in reverse phase sequence constitute negative sequence. The zero sequence components consists of three in-phase vectors. Ignoring the negative sequence components due to load imbalances, no negative and zero sequence components exist in the network during normal (no fault) operation.

Although they are not physically present in the network, monitoring and superimposition of symmetrical quantities can be the basis of understanding the network behaviour during a fault [24,25]. Eqs. (7)–(9) show the measured phase voltages (V_a , V_b , V_c) expressed as a function of the symmetrical components (V^p , V^n , V^z). Similar equations can be written for the currents.

$$V_a = V^p + V^n + V^z \quad (7)$$

$$V_b = a^2 V^p + a V^n + V^z \quad (8)$$

$$V_c = a V^p + a^2 V^n + V^z \quad (9)$$

The complex operator $a = e^{-\frac{3\pi j}{2}}$; subscripts a , b , c indicates the three-phase quantities and the superscripts p , n and z represent the positive, negative and zero sequence components respectively. Using these equations, filters are modelled to resolve the measured phase voltages and line currents into positive, negative and zero sequence vectors. Details regarding modelling of filters are in Appendix B.

3.2. Fault analysis of a network with SOP

MV radial feeders are typically operated with unidirectional power flow. The reverse current in the feeder due to the introduction of SOP could result in a disruption of the protection settings. Therefore the current settings of the relays between the SOP and the fault need recalibration in order to prevent unintended trips of circuit breakers. The detailed fault dynamic response of an SOP is determined by the hardware implementation (e.g. Back-Back VSC or UPFC) and the controller design. Because of its capability of fast response and flexible control, an SOP has a potential to significantly improve fault identification, fault location, fault isolation, and supply restoration [26]. However, the use of SOP brings more complexity to the dynamic response to a fault.

A detailed study of the SOP controller design is required to ensure an improved fault dynamic response of an SOP. In the classical two-level $dq0$ -control used for the back-to-back VSC based SOP, the outer loop attempts to maintain the predefined set points. A change in power flow due to a drop in voltage during AC faults results in an increase in current reference $i_{d Ref}$ and $i_{q Ref}$. The current limiter ensures the maximum rise in the resultant current flowing through the SOP terminals is

limited to i_{max} . The real and reactive power flowing through the SOP terminals during an unbalanced fault remains nearly the same as the pre-fault values. However there are ripples due to voltage imbalance in the feeder, introduced due to the unbalanced fault. In case of a balanced fault the real and reactive power flows drop due to the substantial drop in the feeder voltage [7]. The reactive power flowing through the SOP terminals of the unfaulted feeder remains unchanged. The SOP can continue to provide reactive power support to the unfaulted feeder during a fault on one of the feeders, provided a suitable control for V_{dc} is used. Analysing the dynamic response of the DC link voltage is not in the scope of this paper.

In a conventional distribution network, fault studies are carried out by replacing the fault by a voltage source equal to the pre-fault voltage at the fault point. Symmetrical components are then used to draw equivalent sequence networks by considering the fault point to be the source of imbalance [25]. A low ohmic connection between phases or between phases and earth constitutes a fault [27]. Open circuits and high impedance faults are excluded for this analysis.

In order to enable detailed dynamic fault studies on a network with SOP, the contribution of SOP needs to be included in the sequence networks. During a grid side AC fault, an SOP viewed from the network behaves as a current source. The maximum magnitude of current injected from the SOP during a fault is equal to i_{max} , the physical current limit of the IGBTs. Depending upon the type of fault, positive, negative and zero sequence currents can be injected from the SOP grid connection point. A VSC can produce positive and negative sequence currents using a classical $dq0$ -controller. Zero sequence currents may exist depending on the windings of the isolation transformer. Therefore, the contribution from the SOP is represented by a current source in parallel to their respective sequence component in the equivalent sequence network. The current flowing into the fault is a sum of the current in-ferred from the grid and the current injected from the SOP.

Fig. 4 illustrates the equivalent sequence networks for grid side AC faults on a network with SOP. The portion in the yellow highlights the sequence network of the SOP. f indicates the location of the fault on one of the feeders connected to the SOP terminal. $GCP1$ is the grid connection point of the SOP and the faulted feeder. E_{g1} is the AC grid voltage at G1. Z_{Tg1} represents the AC grid impedance (including the distribution lines and the grid transformer) of the faulted feeder. Z_{Tc1} is the isolation transformer impedance and Z_c is the converter impedance. Superscripts p , n and z represent positive, negative and zero sequence components.

Fig. 4(a) shows the equivalent sequence network for a line-to-ground fault (L_a -G). The positive, negative and zero sequence components are in series for such a fault [25]. Zero sequence components exist in the network only if a ground path is available for the flow of current. The VSC does not produce zero sequence current since it is connected to the delta side of the isolation transformer. However, the fault current at f has a zero sequence component, since the grid transformer and the SOP isolation transformer are star grounded on the feeder side.

Fig. 4(b) shows the equivalent sequence network for an unbalanced line-to-line fault (L_a - L_b). The positive and negative sequence networks are in parallel to each other for an unbalanced fault [25]. Thus, the positive and negative sequence voltages are equal in magnitude. There are no zero sequence components in the network.

The equivalent sequence network for a balanced three-phase fault (L_a - L_b - L_c) is shown in Fig. 4(c). Only the positive sequence current is present in the network. There are no negative and zero sequence currents since the network is balanced. Due to the nature of SOP, the two feeder connected through the SOP are decoupled from each other. Therefore, impedances of unfaulted feeder do not appear in the equivalent sequence network.

4. Detection of fault and fault-index

In a conventional distribution network without DERs, the rotational

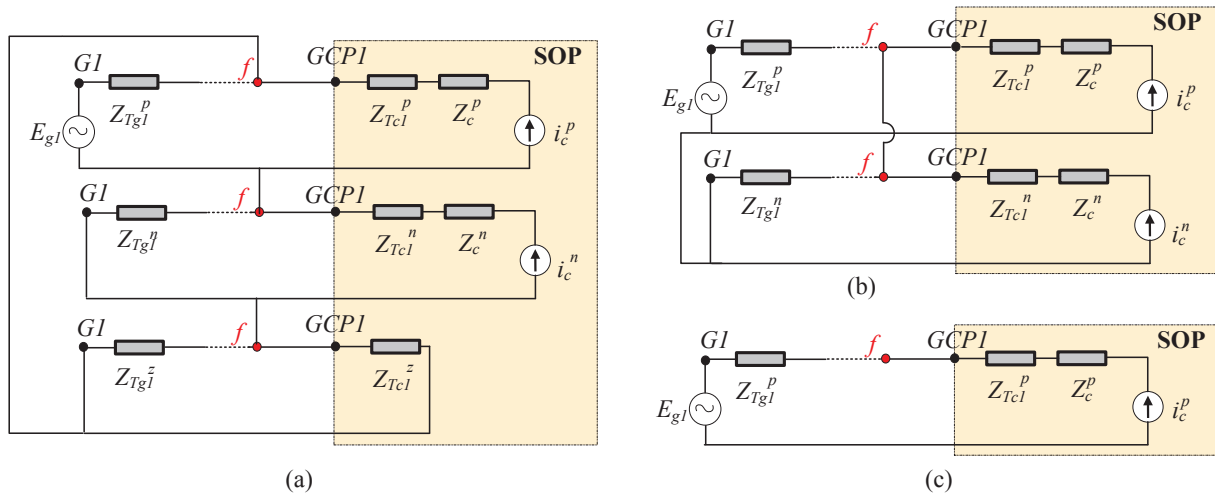


Fig. 4. Equivalent sequence network of AC network and SOP for a fault at point f ; (a) Line-to-ground fault; (b) Line-to-line fault; (c) Three phase fault.

inertia stored in generators is dissipated during a fault in the form of a large fault current. Each type of fault is accurately characterized by the corresponding fault current. Coordination of overcurrent protection devices is achieved by detailed fault analysis carried out on the network.

Measurements of symmetrical current components are introduced as an improvement to the conventional over current measurements. During an unbalanced fault, the negative sequence current is present in a large proportion as compared to load imbalance. Thus, measuring the sequence currents is a good method of fault detection. Authors of [28] defined a function to quantify the negative sequence currents for fault detection. The method eliminates faulty operation of overcurrent protection devices due to transient currents in a network. However, quantification of the negative sequence currents will not be applicable for balanced faults. In addition, the current based detection method in a network with SOP will lead to further complication since SOP contributes sequence currents into faults. Thus, a symmetrical voltage-based method is proposed.

Fault-Index (FI), defined in Eq. (10), is the ratio of the difference between the root mean square (RMS) values of positive, negative and zero sequence voltages to the nominal positive sequence voltage for each phase.

$$FI_x = \frac{(V_{xRMS}^p - (V_{xRMS}^n + V_{xRMS}^z))}{(V_{xRMS}^p(nominal))} \quad (10)$$

x corresponds to phases a, b, c.

The power quality criterion is based on the voltage unbalance factor (VUF). VUF is the ratio of negative to positive sequence voltages. Voltage unbalance may occur in a network due to unbalanced system impedance or due to switching of high loads. They rarely exceed 2%, for a short duration of time. Engineering Recommendation P29 [29] states that the VUF does not go above 1.3% for systems with nominal voltages below 33 kV. To clearly distinguish between voltage imbalance and a fault, an unbalance of 10% or greater ($VUF \geq 0.1$) is assumed to indicate a fault in the network. Using this inequality in Eq. (10), the value of numerator is ≤ 0.9 . Similarly, the value of the denominator can be calculated to be ≥ 1 . Thus, a threshold value of $FI \geq 0.9$ was calculated for a healthy network. Any value of $FI < 0.9$ indicates a fault in the network.

5. Test network

A generic, 11 kV UK distribution network was used in this study [30,31]. The test network consists of two radial feeders connected through a 6 MVA SOP. Each feeder consists of three, 1 km sections.

Fig. 5 shows Feeder-1 of the 11 kV test network connected to Feeder-2 through the SOP. Feeder-2 (not shown in the figure) was modelled identically to Feeder-1 with identical devices and line characteristics. The model was developed in PSCAD/ EMTDC package.

G1 is the grid infeed point. T1 is a 15 MVA, delta-star grid transformer grounded through a 25 Ω resistor on the feeder side. SB1 is an overcurrent based substation circuit breaker. Z_g represents the line impedance of a section. Each 1 km section has a positive (Z_g^p), negative (Z_g^n) and zero (Z_g^z) sequence impedance of $0.164 + j0.082 \Omega$, $0.164 + j0.082 \Omega$ and $0.542 + j0.426 \Omega$ respectively. For simplicity, the positive and negative sequence impedances were assumed equal. L1 and L2 are uniform lumped loads of 1 MW/ph at power factor of 1. The rating of the SOP was selected such that it is sufficient to feed the loads L1 and L2. The isolation transformer (T_{C1}) is a delta-star transformer with a directly grounded star winding on the feeder side. It is connected between the converter terminals (CT1) and the grid connection point (GCP1) on Feeder-1. Z_c ($0.5 + j1.57 \Omega$) represents the impedance of the inductor connected between the converter and the isolation transformer. The converters are connected through a DC link at 35 kV, which consists of two 600 μF capacitors in series. The converter terminals of VSC2 (CT2) are connected to Feeder-2 through an isolation transformer identical to T_{C1} (not shown in the figure).

6. Case studies

The dynamic response of the test network was investigated under various type of faults. Simulations were carried out for the L_a-G , L_a-L_b and $L_a-L_b-L_c$ faults at location f on Feeder-1. A temporary fault occurs at simulation time $t = 1$ s, for a duration of 0.6 s. The duration of the fault was selected less than the time needed for the network protection devices to isolate the fault. Fault resistance was assumed to be negligibly small. Feeder-2 was assumed to be healthy (without fault) throughout the simulation. The network with SOP was studied under three main cases.

Case 1: This case verifies the behaviour of equivalent sequence networks and illustrate their validity for different control schemes of VSC1, under various operating scenarios of the SOP.

The three-phase voltages and currents measured at GCP1 were decomposed into symmetrical components for various faults. The equivalent sequence network developed for each fault was verified by matching the behaviour of measured values to the expected behaviour of their respective sequence network.

The sequence voltages and currents at GCP1 are compared under

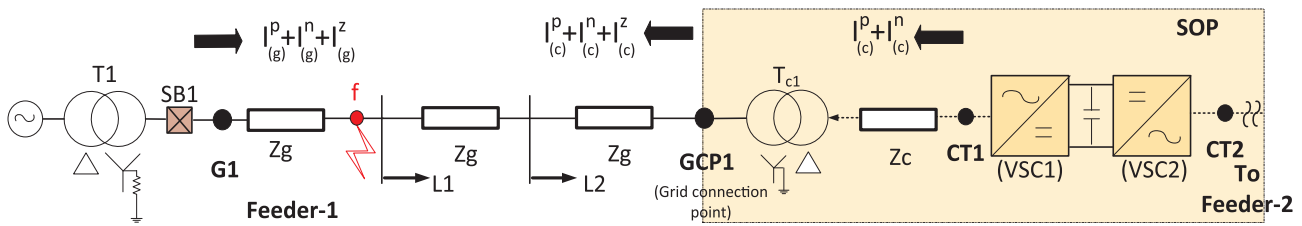


Fig. 5. Generic 11 kV distribution network with SOP (Test network).

Table 1
Symmetrical voltage components (in kV) and FI for two operating mode and various scenarios of SOP operation.

Fault on Feeder 1 @ $t = 1$ s		VSC1 in the P-Q mode				VSC1 in the V_{dc} -Q mode			
		FI	V^p	V^n	V^z	FI	V^p	V^n	V^z
L-G Fault	No power exchange	0.15	4.55	1.62	1.97	0.16	4.47	1.45	2.02
	Q exported to Feeder-1	0.18	4.80	1.64	2.04	0.18	4.72	1.47	2.10
	P imported from Feeder-1 + Q exported to Feeder-1	0.17	4.73	1.64	2.01	0.17	4.61	1.45	2.07
	P and Q exported to Feeder-1^{*,**}	0.17	4.78	1.65	2.06	0.19	4.81	1.49	2.12
L-L Fault	No power exchange	0.05	2.68	2.36	0	0.04	2.84	2.57	0
	Q exported to Feeder-1	0.07	3.06	2.58	0	0.08	3.22	2.68	0
	P imported from Feeder-1 + Q exported to Feeder-1	0.08	3.09	2.57	0	0.06	3.03	2.64	0
	P and Q exported to Feeder-1[*]	0.08	3.12	2.62	0	0.08	3.22	2.71	0
L-L-L Fault	No power exchange	0.01	0.07	0	0	0.01	0.10	0	0
	Q exported to Feeder-1	0.06	0.48	0.07	0	0.06	0.47	0.07	0
	P imported from Feeder-1 + Q exported to Feeder-1	0.06	0.49	0.07	0	0.06	0.48	0.07	0
	P and Q exported to Feeder-1[*]	0.09	0.66	0.09	0	0.08	0.60	0.09	0

* Scenario used for Box plot.
** Scenario used for dynamic analysis of FI.

different control schemes of VSC1 during a fault (i.e. in the P-Q mode and the V_{dc} -Q mode). Extending from Section 2.1, SOP operates in all four coordinates of the P-Q plane. The SOP operates in one of the four possible scenarios during normal (without fault) operating conditions of the network. Each power flow scenario is achievable in the P-Q mode and the V_{dc} -Q mode.

- (1) No power exchange; The SOP is in an ‘open tie-switch’ configuration with no P and Q exchange between Feeder-1 and Feeder-2;
- (2) Q exported to Feeder-1; The SOP operates as a STATCOM providing Q support to the connected feeder (to Feeder-1 in this scenario);
- (3) P imported from Feeder-1 and Q exported to Feeder-1; Q support to Feeder-1 with controlled P transfer from Feeder-1 to Feeder-2;
- (4) P and Q exported to Feeder-1; Q support to Feeder-1 with controlled P transfer from Feeder-2 to Feeder-1 (reverse direction of P flow as compared to Scenario 3).

Q import from the feeder to SOP is not considered. Consumption of Q from the network is detrimental to the voltage profile in a radial distribution network, and hence not recommended.

Fixed set points are used to simulate the above scenarios. Details of the set points for VSC1 and VSC2 are in Appendix C. The measurements were noted for simulation time $t = 1.1$ s such that no transients are present. The sequence voltages and currents for the four scenarios are tabulated. A bar chart for Scenario 4 is used to illustrate the similarities of sequence quantities in the two modes of operation.

Case 2: This case illustrates the reliability of the FI to detect various types of faults

The dynamic response of the FI was analysed for a typical fault. FI was noted for each of the four scenarios in Case 1. The simulations were repeated for different loading conditions to validate FI under different loading conditions. The ability to detect balanced, unbalanced and ground faults was illustrated by comparing FI value to the defined

threshold value. A bar chart was plotted for Scenario 4 to illustrate the similarities of FI during different modes of operation.

Case 3: This case investigates the dependence of the sequence voltages and currents on the SOP set points

The co-relation between the sequence quantities at GCP1 for different $P_{1 Ref}$ and $Q_{1 Ref}$ set points of VSC1 during a fault, when VSC1 is in the P-Q mode, is investigated.

The SOP could operate under any permissible set point prior to a fault. The power transfer through GCP1 during normal (without fault) operation follows the real and reactive power set points. In order to examine the effect of real power set point on the sequence components, simulations are carried out for different values of $P_{1 Ref}$ whilst $Q_{1 Ref}$ equals to zero. $P_{1 Ref}$ is varied from -5 MW to 5 MW in steps of 1 MW. The sequence voltages and currents at GCP1 are analysed.

To analyse the results, the sequence quantities are grouped by the respective sequence. Therefore, the positive sequence voltages (or currents) during the three faults for different values of $P_{1 Ref}$ are grouped in one plot. The negative sequence voltages (or currents) are grouped in the second plot.

Similarly, the effect of reactive power set point is examined by varying $Q_{1 Ref}$ from -5 MVAR to 5 MVAR in steps of 1 MVAR, keeping $P_{1 Ref}$ at zero. The sequence quantities are similarly grouped for analysis.

7. Simulation results

7.1. Case 1

Table 1 shows the values of sequence voltages (in kV) for the four operating scenarios of SOP. The magnitude of sequence voltages observed at GCP1, are consistent with the analytical values of the respective equivalent sequence networks. V^p is maximum for the L_a -G fault and least for the L_a - L_b - L_c fault. V^n is maximum for the L_a - L_b fault. The magnitude of V^p and V^n are nearly equal for the L_a - L_b fault. No V^z is

Table 2
Symmetrical current components (in kA) for two operating mode and various scenarios of SOP operation.

Fault on Feeder 1 @ $t = 1$ s		VSC1 in the P - Q mode			VSC1 in the V_{dc} - Q mode		
		I^p	I^n	I^z	I^p	I^n	I^z
<i>L</i> - <i>G</i> Fault	No power exchange	0.03	0.13	0.90	0.04	0.18	0.92
	<i>Q</i> exported to Feeder-1	0.13	0.14	0.93	0.11	0.19	0.95
	<i>P</i> imported from Feeder-1 + <i>Q</i> exported to Feeder-1	0.17	0.14	0.92	0.16	0.21	0.95
	<i>P</i> and <i>Q</i> exported to Feeder-1*	0.20	0.15	0.93	0.17	0.21	0.96
<i>L</i> - <i>L</i> Fault	No power exchange	0.39	0.44	0	0.36	0.37	0
	<i>Q</i> exported to Feeder-1	0.33	0.46	0	0.30	0.41	0
	<i>P</i> imported from Feeder-1 + <i>Q</i> exported to Feeder-1	0.14	0.40	0	0.1	0.38	0
	<i>P</i> and <i>Q</i> exported to Feeder-1*	0.52	0.44	0	0.51	0.43	0
<i>L</i> - <i>L</i> - <i>L</i> Fault	No power exchange	0.07	0	0	0.09	0	0
	<i>Q</i> exported to Feeder-1	0.72	0.06	0	0.74	0.06	0
	<i>P</i> imported from Feeder-1 + <i>Q</i> exported to Feeder-1	0.71	0.06	0	0.75	0.06	0
	<i>P</i> and <i>Q</i> exported to Feeder-1*	0.74	0.06	0	0.69	0.06	0

present in the L_a - L_b - L_c and L_a - L_b faults. Furthermore, the values are identical for a type of fault in each scenario.

Similarly, Table 2 shows the values of sequence currents (in kA) for the four operating scenarios of SOP. The L_a - L_b - L_c faults are most severe with saturation current flowing through GCP1. During balanced faults, the grid voltage is nearly zero. This gives rise to errors in the computation of θ using PLL, resulting in a non-zero V_q value. Thus, small negative sequence voltage and currents are noted for balanced faults. For the L_a - G fault, I^p and I^n are nearly equal and considerable levels of I^z is present in the network. Although the sequence currents flowing from the grid to the fault point f , remain the same with and without SOP operation. The sequence currents flowing at fault point f , changes due to the introduction of SOP at the end of the feeder.

Fig. 6(a) and (b) compares the sequence voltages for two control modes of SOP. The bar charts illustrate the comparison for Scenario 4. The bars in blue represent voltage at GCP1 when VSC1 in the P - Q mode (VSC2 in the V_{dc} - Q mode) and bars in red represent voltage when VSC1 in the V_{dc} - Q mode (VSC2 in the P - Q mode).

The positive, negative and zero (if applicable) voltages were observed to be nearly equal for both the modes of VSC operation.

Similar observations are made for currents flowing through GCP1. Fig. 7(a) and (b) shows the bar chart comparing currents for the two SOP control modes in Scenario 4. The bars in blue and red represent currents through GCP1 when VSC1 in the P - Q mode (VSC2 in the V_{dc} - Q mode) and when VSC1 is in the V_{dc} - Q mode (VSC2 in the P - Q mode) respectively. Currents from the SOP remain mostly unchanged for both modes of operation, with maximum difference of 0.06 kA between the respective values.

The trends of sequence values observed for various faults are consistent with the expected behaviour based on the equivalent sequence networks. It is clear that sequence networks extending classical fault analysis can be used for a network with connected SOP, regardless of

the control scheme of the VSC connected to the faulted feeder.

7.2. Case 2

Fig. 8(a) shows the dynamic response of the FI for the L_a - G fault in Scenario 4. This scenario was selected as an extreme case, since FI value was highest in this instance. The steady state FI drops well below the threshold value within two cycles (0.04 s) of the fault occurrence. This time does not include the measuring, computation and actuation time needed during real implementation. However, the measurements used for the calculation are available at the SOP controller for its operation and control, thus communication delay is negligible. The firing of the IGBTs can be blocked immediately after the value of FI drops below the threshold. It can be seen from the paper that the computation burden of calculating FI is negligible. Therefore the proposed method is considerably faster than the conventional current based detection method using relay and isolator which usually takes up to thirty cycles (0.6 s) to detect a fault and isolate the SOP [28]. This illustrates the capability of the SOP to detect fault effectively.

The Fault-Index values in each of the four scenarios, under different type of faults are included in Table 1. The validity of FI was further investigated under different loading conditions. The FI was calculated for decreasing loading conditions with 75% and 50% of 1 MW/ph load at 1 and 0.9 power factor. The results are shown in Table 3. The FI varies between 0.15–0.2 for the L_a - G fault, 0.04–0.08 for the L_a - L_b fault and 0.01–0.09 for the L_a - L_b - L_c fault for different operating scenarios of the SOP. The FI was found to be well below the defined threshold of 0.9 for all types of faults, different SOP set points and loading conditions. Fig. 8(b) illustrates the bar chart comparing the FI values for various faults. The red line is the defined threshold value of FI . The values are identical for both control modes. It is clear that FI is a simple and efficient method of fault detection in a distribution network with SOP,

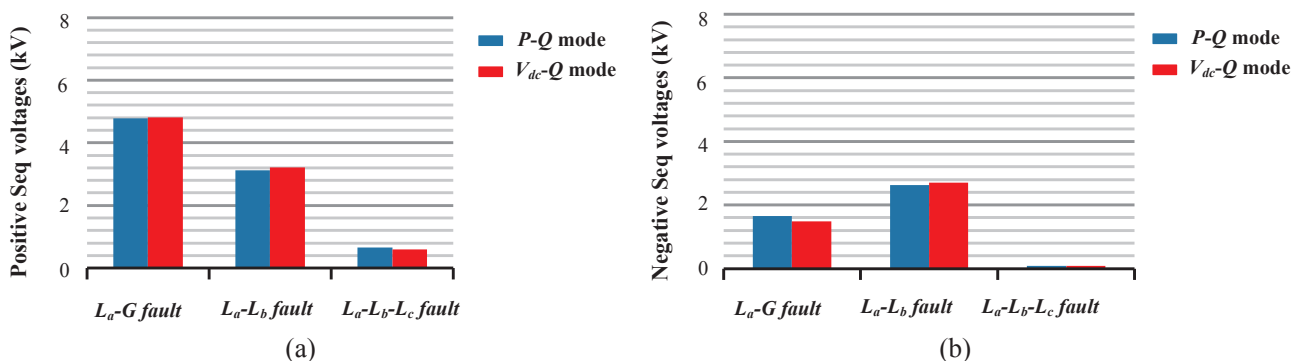


Fig. 6. Comparison of sequence voltages for different control modes of SOP: (a) Positive sequence voltage; (b) Negative sequence voltage.

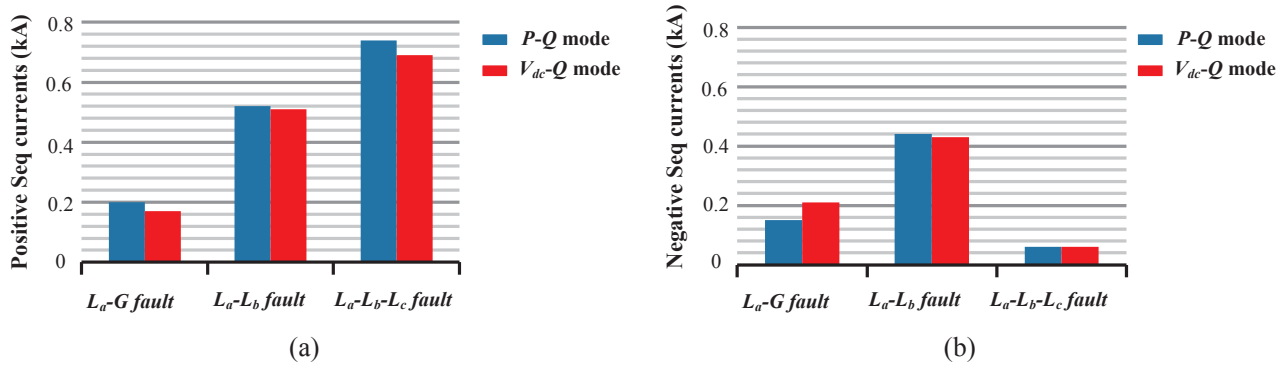


Fig. 7. Comparison of sequence currents for different control modes of SOP: (a) Positive sequence currents; (b) Negative sequence currents.

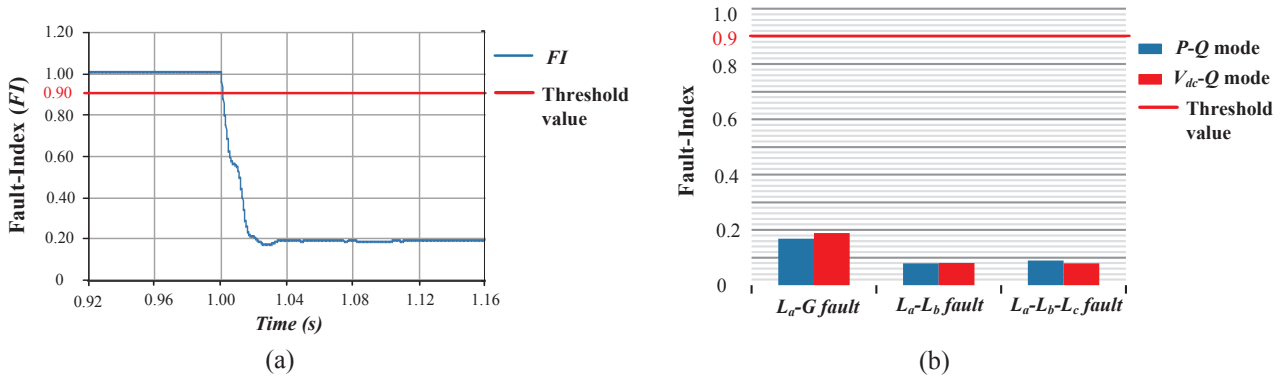


Fig. 8. (a) Dynamic response of FI; (b) Comparison of FI for different control modes of SOP.

without using any additional devices.

7.3. Case 3

In a distribution network, the injection of real and reactive power affects the voltage at the node due to their large R and X ratio [24]. Figs. 9 and 10 exemplifies this behaviour in the test distribution network with SOP. Negative values of the set points indicate injection of power into Feeder-1 from SOP in all the following figures and analysis.

Fig. 9(a) compares the positive sequence voltages for variation of $P_{1 Ref}$ set points and $Q_{1 Ref}$ set points. In the figure the solid line represents

the sequence quantities for range of $P_{1 Ref}$ whilst set point $Q_{1 Ref} = 0$ (marked on lower x-axis and y-axis). Similarly the dotted lines represent the sequence quantities for range of $Q_{1 Ref}$ with set point $P_{1 Ref} = 0$ (marked on upper x-axis and y-axis). The red, blue and black coloured plots indicate the L_a-G , L_a-L_b and $L_a-L_b-L_c$ faults respectively. Fig. 9(b) shows negative sequence with identical representation.

V^p at GCP1 varies linearly based on the pre-fault operating condition of the SOP. It gradually drops with an increase in power exported from Feeder-1 prior to the fault. Conversely, an increase in power injection from SOP to feeder results in a gradual rise of voltage at GCP1. However, in comparison to real power injection, the slope of the

Table 3
FI for various SOP operating scenarios under different loading conditions.

Fault on Feeder 1 @ $t = 1$ s		FI for VSC1 in P-Q mode				FI for VSC1 in V_{dc} -Q mode			
		Per phase loads (L1 and L2) in (MW)							
		0.75 MW @ 1 PF	0.5 MW @ 1 PF	0.75 MW @ 0.9 PF	0.5 MW @ 0.9 PF	0.75 MW @ 1 PF	0.5 MW @ 1 PF	0.75 MW @ 0.9 PF	0.5 MW @ 0.9 PF
L-G Fault	No power exchange	0.15	0.15	0.15	0.15	0.17	0.18	0.17	0.17
	Q exported to Feeder-1	0.16	0.16	0.16	0.16	0.2	0.19	0.19	0.19
	P imported from Feeder-1 + Q exported to Feeder-1	0.15	0.15	0.15	0.15	0.19	0.19	0.18	0.18
	P and Q exported to Feeder-1	0.17	0.17	0.17	0.17	0.2	0.2	0.20	0.20
L-L Fault	No power exchange	0.04	0.03	0.03	0.03	0.03	0.03	0.03	0.03
	Q exported to Feeder-1	0.06	0.06	0.06	0.06	0.06	0.06	0.06	0.06
	P imported from Feeder-1 + Q exported to Feeder-1	0.05	0.05	0.06	0.06	0.05	0.04	0.04	0.04
	P and Q exported to Feeder-1	0.07	0.07	0.07	0.07	0.07	0.07	0.07	0.06
L-L-L Fault	No power exchange	0.01	0.01	0.014	0.01	0.01	0.01	0.01	0.01
	Q exported to Feeder-1	0.06	0.05	0.06	0.05	0.05	0.07	0.05	0.06
	P imported from Feeder-1 + Q exported to Feeder-1	0.06	0.06	0.06	0.06	0.06	0.05	0.06	0.06
	P and Q exported to Feeder-1	0.07	0.07	0.07	0.07	0.07	0.08	0.07	0.07

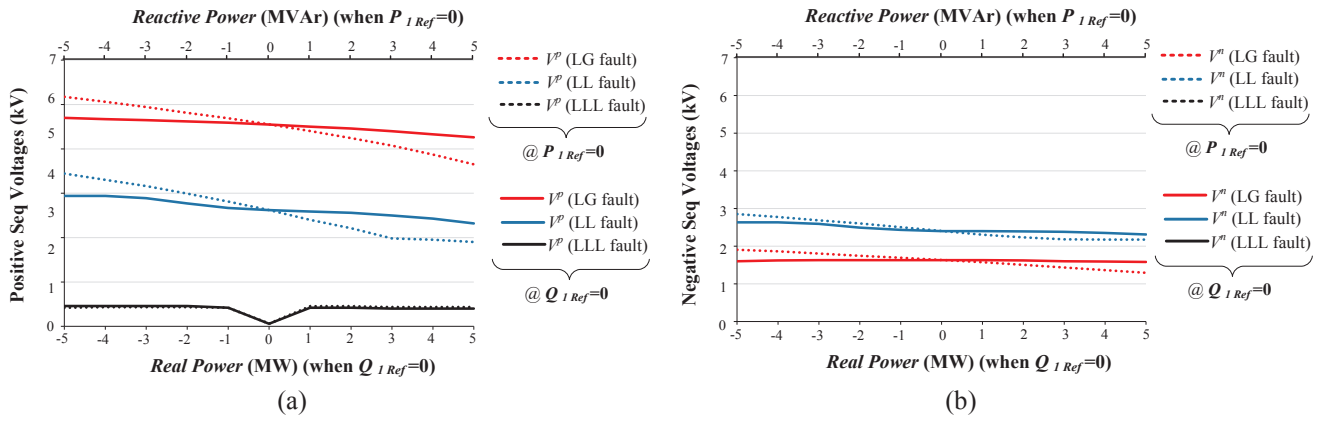


Fig. 9. Sequence voltage for range of $P_{1 Ref}$ set points, $Q_{1 Ref} = 0$ (solid lines); Range of $Q_{1 Ref}$ set points, $P_{1 Ref} = 0$ (Dotted lines). (a) Positive sequence voltages; (b) Negative sequence voltage.

voltage drop is slightly greater for reactive power injection. Fig. 9(b) shows similar results for V^n . Slight droop is observed in variation of negative sequence voltages for changes in $P_{1 Ref}$ and $Q_{1 Ref}$ set points. Similar droop is observed for the zero sequence voltage in the L_a -G fault. However, the percentage variation is very low over the range of set points. Therefore, it is approximated that the negative and the zero sequence voltages at the SOP grid connection point are unaffected by the pre-fault operating condition of SOP during fault analysis on a network with SOP.

In the L_a - L_b - L_c fault, the droop is less evident since the network voltage during the fault is significantly low. It is noteworthy that the terminal voltage is nearly zero for zero set points of SOP, illustrating the open circuit behaviour of the SOP. As illustrated in Case 1, the voltage values depend upon the type of fault and consequently upon the equivalent sequence network connection. However, regardless of the type of fault, the trend of voltage variation is consistent for corresponding change in real and reactive power flow through the SOP terminals.

Fig. 10(a) and (b) shows the positive and negative sequence currents with variation of the $P_{1 Ref}$ and $Q_{1 Ref}$ set points. For the L_a -G fault there is a steep, linear rise in the magnitude of the currents with rise in $P_{1 Ref}$ and $Q_{1 Ref}$ regardless of the direction of power flow prior to the fault. In contrast to the L_a -G fault the sequence currents in the L_a - L_b fault has a nonlinear relation to the set points. In addition, the variation in currents for changes in $P_{1 Ref}$ and $Q_{1 Ref}$ shows dependence on the polarity of set points and appears converse to each other.

For the L_a - L_b - L_c fault, the currents are largely uniform and unaffected by changes in set points (for non-zero set points). For zero set

point, the behaviour of SOP is consistent with an open circuit with no current flowing through the SOP.

The variation of currents with changes in set points is similar for a given type of fault, but varies considerably for different type of faults. Unlike the sequence voltages, the sequence current injection shows a nonlinear dependency to the pre-fault condition. Further investigation is required to generalize the current response of the SOP under different faults. However, this clearly illustrates the need for a non-current based method for fault detection at the grid connection point of the SOP.

8. Conclusions

The dynamic performance of a medium voltage distribution network with SOP was investigated, under grid side AC faults. Conventional fault analysis technique using sequential network was extended to include SOP. Equivalent sequence networks were developed for a network with an SOP under a line-ground fault, a line-to-line unbalanced fault and a three-phased balanced fault. Equivalent sequential networks were drawn by combining the sequence components of the network with the contribution from the SOP. Fault analysis using this representation was validated on a generic distribution network with connected SOP. The sequence voltage values at the SOP grid connection point were found to be consistent and predictable for different operating scenarios whilst operating within the physical limits of SOP. In addition, the sequence voltages were identical for both P - Q and V_{dc} - Q modes of SOP operation.

The FI , defined using the positive and the negative sequence components of the voltage at the grid connection points of the SOP, was

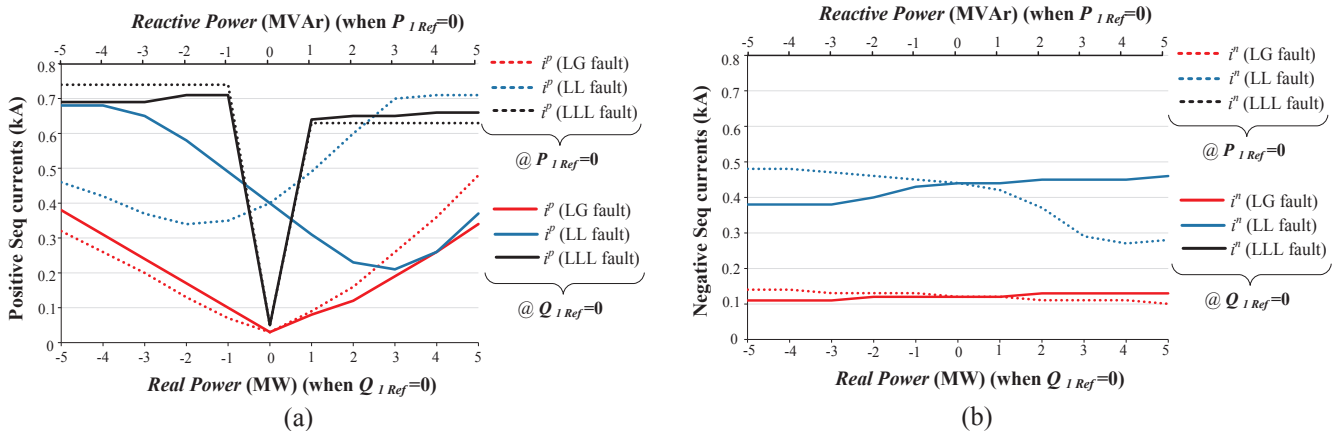


Fig. 10. Sequence current for range of $P_{1 Ref}$ set points, $Q_{1 Ref} = 0$ (solid lines); Range of $Q_{1 Ref}$ set points, $P_{1 Ref} = 0$ (Dotted lines). (a) Positive sequence currents; (b) Negative sequence currents.

Table 4
The set points used to simulate Scenarios 1–4 in Case 1.

Scenario No	VSC1 ($P_{1 Ref}$ $Q_{1 Ref}$) & VSC2 (V_{dc} Ref $Q_2 Ref$) (MW, MVar) (kV, MVar)	VSC1 ($V_{dc Ref}$ $Q_{1 Ref}$) & VSC2 (P_2 Ref $Q_2 Ref$) (kV, MVar) (MW, MVar)
1	(0, 0) (35, 0)	(35, 0) (0, 0)
2	(0, -2) (35, 0)	(35, -2) (0, 0)
3	(2, -2) (35, 0)	(35, -2) (2, 0)
4	(-2, -2) (35, 0)	(35, -2) (-2, 0)

Power flowing from SOP to Feeder-1 and Feeder-2 to SOP is assumed positive.

found to be effective for AC fault detection in a network. The *FI* quantifies the unbalance in the network normalized by the nominal voltage. The consistent behaviour of sequence voltages in the network make them reliable for fault detection. Currently, *FI* cannot determine the type of fault on its own. However, *FI* and its relationship with the sequence networks can be utilized to develop the capability of the SOP to identify different types of faults.

A better understanding of the relationship between the sequence currents injected during a fault and the network conditions is needed to achieve proper over-current co-ordination. Each fault type needs to be analysed individually. This is important to understand the impact of introducing an SOP to a network with existing protection settings and

feeder automation devices.

Acknowledgements

The authors gratefully acknowledge the Angle-DC project, UK/India HEAPD project (Grant No. EP/K036211/1) and FLEXIS project. FLEXIS is part-funded by the European Regional Development Fund (ERDF), through the Welsh Government. Information on the data underpinning the results presented here, including how to access them, can found in the Cardiff University data catalogue at <http://doi.org/10.17035/d.2017.0040699004>.

Appendix A

The Park transformation matrix $T(\theta)$ is

$$T(\theta) = \begin{bmatrix} \cos(\theta) & \cos(\theta - \frac{2\pi}{3}) & \cos(\theta + \frac{2\pi}{3}) \\ \sin(\theta) & \sin(\theta - \frac{2\pi}{3}) & \sin(\theta + \frac{2\pi}{3}) \\ 1/2 & 1/2 & 1/2 \end{bmatrix}$$

Appendix B

$$V_x = v_x^p + v_x^n + v_x^z;$$

where $v_x = [v_a \ v_b \ v_c]^T$;

$$\begin{bmatrix} v_a \\ v_b \\ v_c \end{bmatrix} = \begin{bmatrix} v_a^p & v_a^n & v_a^z \\ v_b^p & v_b^n & v_b^z \\ v_c^p & v_c^n & v_c^z \end{bmatrix} \begin{bmatrix} 1 \\ 1 \\ 1 \end{bmatrix}$$

$$\begin{bmatrix} v_a^p \\ v_b^p \\ v_c^p \end{bmatrix} = \frac{1}{3} \begin{bmatrix} 1 & 1/2 & 1/2 \\ 1/2 & 1 & 1/2 \\ 1/2 & 1/2 & 1 \end{bmatrix} \begin{bmatrix} v_a \\ v_b \\ v_c \end{bmatrix} - \frac{1}{j2\sqrt{3}} \begin{bmatrix} 0 & 1 & -1 \\ -1 & 0 & 1 \\ 1 & -1 & 0 \end{bmatrix} \begin{bmatrix} v_a \\ v_b \\ v_c \end{bmatrix}$$

$$\begin{bmatrix} v_a^n \\ v_b^n \\ v_c^n \end{bmatrix} = \frac{1}{3} \begin{bmatrix} 1 & 1/2 & 1/2 \\ 1/2 & 1 & 1/2 \\ 1/2 & 1/2 & 1 \end{bmatrix} \begin{bmatrix} v_a \\ v_b \\ v_c \end{bmatrix} + \frac{1}{j2\sqrt{3}} \begin{bmatrix} 0 & 1 & -1 \\ -1 & 0 & 1 \\ 1 & -1 & 0 \end{bmatrix} \begin{bmatrix} v_a \\ v_b \\ v_c \end{bmatrix}$$

Appendix C

See Table 4.

References

[1] Kim M, Bae S. Decentralized control of a scalable photovoltaic (PV)-battery hybrid power system. *Appl Energy* 2017;188:444–55. <http://dx.doi.org/10.1016/j.apenergy.2016.12.037>.
 [2] Green T, Jenkins N. HubNet position paper no 3 – issues for distribution system operation at 2030 – version 4.0; 2014. <http://hubnet.org.uk/filebid/523/2030GridOperation.pdf> [accessed 27 January 2017].
 [3] Silversildes R, Green T, Luth T. HubNet position paper no 6 – power electronics in

distribution system management - version 2.0; 2015. p. 1–21. http://hubnet.org.uk/filebid/535/PE_Distribution.pdf [accessed 27 January 2017].
 [4] Wang C, Song G, Li P, Ji H, Zhao J, Wu J. Optimal siting and sizing of soft open points in active electrical distribution networks. *Appl Energy* 2017;189:301–9. <http://dx.doi.org/10.1016/j.apenergy.2016.12.075>.
 [5] Bloemink JM, Green TC. Benefits of distribution-level power electronics for supporting distributed generation growth. *IEEE Trans Power Deliv* 2013;28:911–9. <http://dx.doi.org/10.1109/TPWRD.2012.2232313>.
 [6] Bloemink JM, Green TC. Increasing photovoltaic penetration with local energy storage and soft normally-open points. 2011 IEEE Power Energy Soc. Gen. Meet.

- Detroit, USA; 2011. p. 1–8. 10.1109/PES.2011.6039561.
- [7] Cao W, Wu J, Jenkins N, Wang C, Green T. Operating principle of Soft Open Points for electrical distribution network operation. *Appl Energy* 2016;164:245–57. <http://dx.doi.org/10.1016/j.apenergy.2015.12.005>.
- [8] Cao W, Wu J, Jenkins N. Feeder load balancing in MV distribution networks using soft normally-open points. *IEEE PES innov smart grid technol Eur. Istanbul, Turkey; 2014*. p. 1–6. 10.1109/ISGTEurope.2014.7028874.
- [9] Cao W, Wu J, Huang Z. Use of soft open points for supply restoration in medium voltage distribution networks. *IEEE PES Asia-Pacific power energy eng conf, Brisbane, Aust.; 2015*. p. 1–6.
- [10] Bloemink JM, Green TC. Increasing distributed generation penetration using soft normally-open points. *IEEE PES gen meet, USA; 2010*. p. 1–8. 10.1109/PES.2010.5589629.
- [11] Cao W, Wu J, Jenkins N, Wang C, Green T. Benefits analysis of Soft Open Points for electrical distribution network operation. *Appl Energy* 2016;165:36–47. <http://dx.doi.org/10.1016/j.apenergy.2015.12.022>.
- [12] Long C, Wu J, Thomas L, Jenkins N. Optimal operation of soft open points in medium voltage electrical distribution networks with distributed generation. *Appl Energy* 2016;184:427–37. <http://dx.doi.org/10.1016/j.apenergy.2016.10.031>.
- [13] Aithal A, Long C, Cao W, Wu J, Ugalde-Loo CE. Impact of soft open point on feeder automation. *IEEE int energy conf (ENERGYCON), Leuven, Belgium; 2016*. 10.1109/ENERGYCON.2016.7514101.
- [14] Scottish Power Energy Networks. Electricity NIC submission: SP energy networks – ANGLE-DC; 2016. <https://www.ofgem.gov.uk/publications-and-updates/electricity-nic-submission-sp-energy-networks-angle-dc> [accessed 15 December 2016].
- [15] LCN Fund Tier 2 Bid 2014 low carbon networks fund full submission pro-forma section 1 : project summary; 2014. https://www.ofgem.gov.uk/sites/default/files/docs/2013/11/lcnf_submission_from_sp_distribution_-_ace_0.pdf [accessed 27 January 2017].
- [16] Candelaria J, Park JD. VSC-HVDC system protection: a review of current methods. 2011 IEEE/PES power syst conf expo PSCE 2011; 2011. p. 1–7. 10.1109/PSCE.2011.5772604.
- [17] Barragán-Villarejo M, Romero-Ramos E, Marano-Marcolini A, Maza-Ortega J, Gómez-Expósito A. Voltage source converter-based topologies to further integrate renewable energy sources in distribution systems. *IET Renew Power Gener* 2012;6:435–45. <http://dx.doi.org/10.1049/iet-rpg.2011.0246>.
- [18] Yazdani A, Iravani R. Grid imposed frequency VSC system: control in dq-frame. *Voltage-sourced convert. Power Syst Model Control Appl*. John Wiley & Sons; 2010. p. 204–45.
- [19] Trujillo CL, Velasco D, Guarnizo JG, Díaz N. Design and implementation of a VSC for interconnection with power grids, using the method of identification the system through state space for the calculation of controllers. *Appl Energy* 2011;88:3169–75. <http://dx.doi.org/10.1016/j.apenergy.2011.02.038>.
- [20] Kalantar M, Mousavi GSM. Dynamic behavior of a stand-alone hybrid power generation system of wind turbine, microturbine, solar array and battery storage. *Appl Energy* 2010;87:3051–64. <http://dx.doi.org/10.1016/j.apenergy.2010.02.019>.
- [21] Egea Álvarez A, Junyent Ferré A, Gomis Bellmunt O. Active and reactive power control of grid connected distributed generation systems. *Model Control Sustain Power Syst: Springer, Berlin Heidelberg; 2012*. p. 47–81.
- [22] Teodorescu R, Liserre M, Rodriguez P. Grid converters for photovoltaic and photovoltaic and wind power systems John Wiley & Sons; 2011. <http://dx.doi.org/10.1002/9780470667057>.
- [23] Fortescue BYC. The measurement of power in polyphase circuits. *J Am Inst Electr Eng* 1923;42:205–18.
- [24] Weedy BM, Cory BJ, Jenkins N, Ekanayake JB, Strbac G. *Electric power systems*. 5th ed. Wiley; 2012.
- [25] ALSTOM Grid. Network protection & automation guide; 2011. p. 336–51. <http://electrical-engineering-portal.com/download-center/books-and-guides/electrical-engineering/automation-guide> [accessed 22 December 2016].
- [26] Tang C-Y, Chen Y-F, Chen Y-M, Chang Y-R. DC-link voltage control strategy for three-phase back-to-back active power conditioners. *IEEE Trans Ind Electron* 2015;62:6306–16. <http://dx.doi.org/10.1109/TIE.2015.2420671>.
- [27] Plet CA, Green TC. Fault response of inverter interfaced distributed generators in grid-connected applications. *Electr Power Syst Res* 2014;106:21–8. <http://dx.doi.org/10.1016/j.epsr.2013.07.013>.
- [28] Lotfi-fard S, Faiz J, Iravani MR. Improved overcurrent protection using symmetrical components. *IEEE Trans Power Deliv* 2007;22:843–50. <http://dx.doi.org/10.1109/TPWRD.2007.893591>.
- [29] The Electricity Council. Planning limits for voltage unbalance in the United Kingdom. *Eng Recomm P29; 1990*. p. 8. <http://www.nienetworks.co.uk/documents/Security-planning/ER-P29.aspx> [accessed 27 January 2017].
- [30] Foote C, Djapic P, Ault G, Mutale J, Strbac G. United kingdom generic distribution system (UKGDS). DTI Cent Distrib Gener Sustain Electr Energy; 2010. <https://github.com/sedg/ukgds> [accessed 27 January 2017].
- [31] Ingram S, Probert S, Jackson K. Impact of small scale embedded generation on operating parameters of distribution networks. Department of Trade and Industry & Renewable Energy Program. K/El/00303/04/01 URN 03/1051; 2003. http://webarchive.nationalarchives.gov.uk/20100919181607/www.ensg.gov.uk/assets/22_01_2004_phase1b_report_v10b_web_site_final.pdf [accessed 27 January 2017].